Article

Discovery Medicine 2025; 37(198): 1263–1273
https://doi.org/10.24976/Discov.Med.202537198.111

DTX3L Promotes Intrahepatic Cholangiocarcinoma Progression Through P53 Ubiquitination-Mediated Inhibition of ER Stress and Apoptosis

Haoming Lan[1,†], Jun Hu[1,†], Linsheng Huang[1], Xianfeng Sheng[1], Meng Zhou[1], Shuo Yang[2,*], Gan Zhang[1,*]

[1]Department of Hepatopancreatobiliary Surgery, Taihe Hospital, Hubei University of Medicine, 442000 Shiyan, Hubei, China
[2]Department of Ultrasound Medicine, Taihe Hospital, Hubei University of Medicine, 442000 Shiyan, Hubei, China
*Correspondence: 13581366066@163.com (Shuo Yang); zhanggan0101@163.com (Gan Zhang)
[†]These authors contributed equally.
Published: 20 July 2025

Background: Deltex E3 ubiquitin ligase 3L (DTX3L) is implicated in the progression of various cancer types; however, its specific contribution to intrahepatic cholangiocarcinoma (ICC) remains unexplored. Therefore, this study sought to investigate the involvement of DTX3L in ICC development and elucidate its regulatory effect on endoplasmic reticulum stress (ERS) and apoptosis via P53 ubiquitination.

Methods: We systematically evaluated DTX3L expression in ICC samples using qRT-PCR and Western blotting. Functional assays, including Cell Counting Kit-8 (CCK-8), colony formation, Terminal deoxynucleotidyl transferase dUTP nick end labeling (TUNEL), and flow cytometry, were performed to assess cell proliferation and apoptosis. Co-immunoprecipitation and ubiquitination assays were employed to investigate the interaction between DTX3L and P53. *In vivo*, tumor xenograft models were used to examine the effects of DTX3L knockdown on tumor growth and ERS pathway activation.

Results: DTX3L was significantly overexpressed in ICC tissues and cells ($p < 0.05$), and its overexpression promoted proliferation, suppressed apoptosis, and downregulated ERS-associated markers, including phosphorylated eukaryotic initiation factor 2 alpha (p-eIF2α), protein kinase R-like endoplasmic reticulum kinase (PERK), C/EBP homologous protein (CHOP), and activating transcription factor 4 (ATF4) ($p < 0.01$). Mechanistically, DTX3L directly interacted with P53 and enhanced its ubiquitination and degradation, attenuating its tumor-suppressive effects. Knockdown of DTX3L significantly activated ERS signaling and induced apoptosis ($p < 0.01$), the effects were reversed by simultaneous P53 knockdown ($p < 0.01$).

Conclusion: DTX3L is a critical oncogene in ICC progression by promoting P53 ubiquitination-mediated suppression of ERS and apoptosis. These findings suggest that DTX3L may serve as a promising therapeutic target in ICC.

Keywords: intrahepatic cholangiocarcinoma; DTX3L; P53; ubiquitination; endoplasmic reticulum stress

Introduction

Intrahepatic cholangiocarcinoma (ICC) is a malignant tumor originating from the epithelial cells of the intrahepatic bile duct, known for its aggressive behavior and high malignancy. Over the recent years, its incidence has gradually increased globally, particularly in Asia and some parts of the West, making ICC as a significant threat to public health [1,2]. Epidemiological studies indicate that ICC is the second most prevalent primary liver cancer, after hepatocellular carcinoma, with significantly rising mortality and morbidity rates. Its prognosis remains unfavorable, with a 5-year survival rate typically below 20% [3,4]. Currently, surgical resection remains the preferred treatment option for ICC. Nevertheless, owing to its highly invasive nature and early intrahepatic metastasis, most patients presented at an unresectable stage. Additionally, adjuvant treatments like targeted agents, chemotherapy, and immunotherapy offer limited benefits, and no consensus on standardized therapeutic regimens has been achieved [5,6]. Therefore, investigating the underlying molecular mechanisms and identifying potential therapeutic approaches for ICC are critical to improving patient outcomes.

Tumor initiation and progression involve a series of complex biological processes, including genetic mutations, aberrant signaling pathways, and remodeling of the tumor microenvironment. The tumor suppressor gene—P53 plays a crucial role in preserving genomic integrity by managing the cell cycle, promoting apoptosis, and facilitating DNA damage repair [7]. However, in the majority of cancer types, compromised P53 function or its aberrant degradation is the fundamental driver of malignancy. Studies suggest that P53 is primarily degraded via the ubiquitin-proteasome mechanism, and aberrant activation of this pro-

cess contributes significantly to tumorigenesis [8,9]. Ubiquitination is mediated by the coordinated actions of E1 (ubiquitin-activating enzyme), E2 (ubiquitin-conjugating enzyme), and E3 (ubiquitin ligase), with E3 ligases determining substrate specificity [10,11]. Aberrant activation of the ubiquitination pathway leads to excessive degradation of P53, thereby impairing its tumor-suppressive functions.

Furthermore, endoplasmic reticulum stress (ERS), a critical response to an imbalance in intracellular homeostasis, is closely linked to cancer development [12,13]. ERS signaling can mediate cell death through factors like C/EBP homologous protein (CHOP) or promote cytoprotection through the protein kinase R-like endoplasmic reticulum kinase (PERK)–eukaryotic initiation factor 2 alpha (eIF2α)–activating transcription factor 4 (ATF4) axis; however, its precise role in ICC pathobiology remains controversial [14,15]. Some studies reveal that P53 may induce tumor cell apoptosis by regulating ERS pathway, while dysregulated ERS could synergize with P53 loss to accelerate cancer progression [16]. However, the specific interaction mechanisms between P53 and ERS in ICC remain unclear.

Deltex E3 ubiquitin ligase 3L (DTX3L), a member of the E3 ubiquitin ligase family, is involved in DNA damage repair, chromatin remodeling, and regulation of protein stability [17]. DTX3L has been reported to drive tumor cell proliferation and inhibit apoptosis in multiple malignancies, including breast, cervical, and brain cancers, primarily through ubiquitin-mediated protein degradation [18,19]. However, its function in ICC, particularly in the context of P53 stability and ERS regulation, remains undefined. Given the crucial role of E3 ligases in modulating P53 degradation and the emerging significance of P53-ERS signaling in tumor progression, we hypothesized that DTX3L serves as a key upstream regulator within this axis.

In this study, we aimed to investigate the role of DTX3L in ICC and its regulatory impact on ERS and apoptosis through the modulation of P53 ubiquitination. Employing comprehensive *in vitro* cellular assays and *in vivo* animal experiments, we sought to elucidate a novel DTX3L–P53–ERS signaling axis, thereby expanding our understanding of ICC's molecular pathogenesis, and identifying DTX3L as a potential therapeutic target.

Materials and Methods

Tissue Collection

Tumor tissues (ICC group) and adjacent non-tumorous tissues (Normal group) were collected from 10 patients with histologically confirmed ICC who underwent surgical resection at Taihe Hospital, Hubei University of Medicine (Shiyan, China) between March 2023 and December 2023. Inclusion criteria for patient recruitment included (1) histopathologically confirmed ICC; (2) no preoperative chemotherapy or radiotherapy; and (3) availability of paired tumor and adjacent normal tissues. However, patients with mixed-type primary liver cancer, history of other malignancies, or incomplete clinical or pathological data were excluded. Based on the American Joint Committee on Cancer (AJCC, 8th edition) pathological staging system, 6 cases were assigned to stage II and 4 to stage III [20].

Cell Culture and Transfection

Normal human intrahepatic biliary epithelial cells (HIBECs, #CP-H042, Procell, Wuhan, China) and ICC cells (RBE, #CL-0191, Procell, Wuhan, China) were cultured in RPMI-1640 medium (#11875093, Gibco, Thermo Fisher Scientific, Waltham, MA, USA) supplemented with 10% fetal bovine serum (FBS, #A5670701, Gibco, Thermo Fisher Scientific, Waltham, MA, USA) and 1% penicillin-streptomycin (PSS, #15140148, Gibco, Thermo Fisher Scientific, Waltham, MA, USA), and incubated at 37 °C with 5% CO_2. Each cell line underwent authentication using short tandem repeat (STR) profiling, exhibited typical morphology upon microscopic examination, and was tested for mycoplasma contamination before use.

DTX3L was selected as the gene of interest based on its role as an E3 ubiquitin ligase and involvement in tumor growth [18]. To assess regulatory function of DTX3L in ICC, RBE cells were divided into five experimental sets: (1) oeNC group: RBE cells transfected with negative control pcDNA3.1; (2) oe-DTX3L group: RBE cells transfected with pcDNA3.1-DTX3L; (3) shNC group: RBE cells transfected with negative control shRNA; (4) sh-DTX3L group: RBE cells transfected with DTX3L-specific shRNA; and (5) sh-DTX3L+sh-P53 group: RBE cells co-transfected with shRNAs targeting DTX3L and P53.

All shRNA constructs were acquired from GenePharma (Shanghai, China). The targeting sequences used were as follows: sh-DTX3L: 5′-GCATCAACATGAAGGACATAT-3′; sh-P53: 5′-GCGGAACTCGAATTCATTTCT-3′; and shNC: 5′-TTCTCCGAACGTGTCACGT-3′.

For overexpression, full-length human DTX3L cDNA was cloned into the pcDNA3.1(+) expression vector (Invitrogen, Carlsbad, CA, USA) and verified by Sanger sequencing. Cellular transfections were performed using Lipofectamine™ 3000 (Thermo Fisher Scientific, Waltham, MA, USA) according to the manufacturer's protocol. For each well of a 6-well plate, 2.5 µg of plasmid DNA was mixed with 5 µL of Lipofectamine 3000 reagent. Cells were incubated with the transfection mixture for 6 hours, after which the medium was refreshed. After that, cells were harvested 48 hours of post-transfection for subsequent analyses.

Xenograft Tumor Model and In Vivo Experimental Procedures

A total of 24 BALB/c nude mice (male, 20 ± 2 g, weighting six weeks old) were obtained from Charles

Table 1. Primers used in qRT-PCR.

Gene	Forward primer (5′-3′)	Reverse primer (5′-3′)
DTX3L	CCCGAGTACGAAGGAAGCTG	CACTCTCTCCTTAGCTGCCC
GAPDH	GTCTCCTCTGACTTCAACAGCG	ACCACCCTGTTGCTGTAGCCAA

DTX3L, Deltex E3 ubiquitin ligase 3L; *GAPDH*, glyceraldehyde-3-phosphate dehydrogenase.

River Inc. (Beijing, China) and maintained under specific pathogen-free (SPF) conditions with controlled temperature (22 ± 2 °C), humidity (55 ± 5%), and a 12-hour light/dark cycle. Mice had unrestricted access to autoclaved food and water throughout the experiment.

Mice were randomly divided into four groups (n = 6 for each group), as described below: (1) oeNC group: mice injected with RBE cells transfected with empty vector (pcDNA3.1); (2) oe-DTX3L group: mice injected with RBE cells overexpressing DTX3L (pcDNA3.1-DTX3L); (3) shNC group: mice injected RBE cells carrying negative control shRNA; (4) sh-DTX3L group: mice injected with DTX3L-knockdown cells (shRNA).

Each mouse received a subcutaneous injection of 5×10^6 RBE cells suspended in 100 µL of a 1:1 phosphate-buffered saline (PBS, #21-040-CV, Corning, Corning, NY, USA) and Matrigel suspension (#354234, Corning, Corning, NY, USA) into the right dorsal flank. Tumor formation was initially assessed by palpation on day 4 post-injection, with successful modeling defined as a palpable mass exceeding 50 mm^3 within 7 days. After that, tumor dimensions were recorded every four days utilizing digital calipers, and volume was computed as (length × $width^2$)/2.

Mice were observed daily for signs of ulceration or distress. On day 28 after injection, all mice were euthanized through CO_2 asphyxiation, with cervical dislocation used to confirm death. Tumors were excised, photographed alongside a calibrated ruler, and weighed. Samples were then either snap-frozen in liquid nitrogen or fixed in 4% paraformaldehyde for subsequent analyses.

Quantitative Real-Time PCR (qRT-PCR)

Total RNA was isolated from ICC tumor tissues (ICC group), adjacent normal tissues (Normal group), ICC cells (RBE), and normal HIBECs using Trizol reagent (#15596018CN, Thermo Fisher Scientific, Waltham, MA, USA). After chloroform-assisted phase separation, isopropanol-mediated precipitation, and rinsing with 75% ethanol, RNA concentration and purity (optical density (OD)260/OD280 between 1.8 and 2.0) were determined using a NanoDrop spectrophotometer (Thermo Fisher Scientific, Waltham, MA, USA). After that, RNA (1 µg) was reverse-transcribed into cDNA. DTX3L specific primers were used (Table 1) for qRT-PCR with SYBR Green detection. The amplification procedure consisted of an initial denaturation at 95 °C for 3 minutes, followed by 40 cycles of 95 °C for 15 seconds and 60 °C for 30 seconds (annealing/extension), concluding with a melting curve analysis to confirm primer specificity. Gene expression levels were quantified using the ΔΔCt method. ΔCt value was calculated as the difference between the target and internal reference gene Ct values, and ΔΔCt as the difference between experimental and control ΔCt values. Relative expression levels were expressed as $2^{-\Delta\Delta Ct}$.

CCK-8 Assay

Logarithmic-phase RBE cells from the oeNC, oe-DTX3L, shNC, sh-DTX3L, and sh-DTX3L+sh-P53 groups were seeded at a density of 5×10^3 cells/well in 96-well plates, with five replicates per group and blank medium wells serving as controls. After 12, 24, 48, and 72 hours of incubation, 10 µL of Cell Counting Kit-8 (CCK-8) reagent (#C0037, Beyotime Biotechnology, Shanghai, China) was added to each well. Following a 2-hour incubation at 37 °C, the absorbance (OD value) at 450 nm was measured using a microplate reader (BioTek, ELx800, Winooski, VT, USA). Finally, cell viability was determined as the mean OD450 for each group, and proliferation curves were plotted accordingly.

Cell Colony Formation Assay

Log-phase RBE cells from each group were cultured in 6-well plates at 500 cells per well, with three replicate wells per group. Cells were incubated in RPMI-1640 medium supplemented with 10% FBS and 1% PSS for 14 days to form visible colonies (≥50 cells per colony). After two PBS washes, the samples were fixed for 20 minutes in 4% paraformaldehyde (#P0099, Beyotime Biotechnology), followed by 15-minute staining with 0.1% crystal violet (#C0121, Beyotime Biotechnology, Shanghai, China). After air drying, colonies were imaged and counted using an inverted microscope (Olympus CKX53, Tokyo, Japan).

TUNEL Assay

Apoptosis was assessed using a terminal deoxynucleotidyl transferase dUTP nick end labeling (TUNEL) assay kit (#C1086, Beyotime Biotechnology, Shanghai, China). Samples were fixed in 4% paraformaldehyde for 30 minutes, followed by permeabilization in 0.1% Triton X-100 for 10 minutes at ambient temperature. After three PBS washes, slides were treated with a mixture of terminal deoxynucleotidyl transferase (TdT) enzyme and fluorescein-labeled dUTP (e.g., FITC-dUTP or Alexa Fluor-dUTP) was placed onto the slides and maintained at 37 °C for 1 hour in the dark. Following thorough washing, samples were stained with 4′,6-diamidino-2-phenylindole (DAPI,

#C1002, Beyotime Biotechnology, Shanghai, China) and mounted using an antifade medium. Finally, slides were observed, and images were recorded using an Olympus IX73 fluorescence microscope (Tokyo, Japan). For each of the three independent replicates, five randomly selected microscopic fields were analyzed, and the apoptotic rate (%) was calculated as (TUNEL-positive nuclei/total nuclei) $\times$ 100.

Western Blot Analysis

Total protein was extracted using radioimmunoprecipitation assay (RIPA) lysis buffer (#P0013C, Beyotime Biotechnology, Shanghai, China), containing protease and phosphatase inhibitors. Protein concentration was determined using a bicinchoninic acid (BCA) Protein Assay Kit (#P0012, Beyotime Biotechnology, Shanghai, China). Equal amounts (30 µg) of each protein were resolved by sodium dodecyl sulfate–polyacrylamide gel electrophoresis (SDS-PAGE) and subsequently transferred onto polyvinylidene fluoride (PVDF) membranes (IPVH00010, Millipore, Burlington, MA, USA). Membranes were blocked in 5% skim milk for 2 hours at room temperature, then incubated overnight at 4 °C with primary antibodies, including DTX3L (1:2000, ab70621, Abcam, Cambridge, UK), P53 (1:1000, ab26, Abcam, Cambridge, UK), Bcl-2 (1:1000, ab182858, Abcam, Cambridge, UK), Bax (1:1000, ab182733, Abcam, Cambridge, UK), Cleaved Caspase-3 (1:500, ab32042, Abcam, Cambridge, UK), Cleaved poly (ADP-ribose) polymerase (Cleaved PARP, 1:1000, ab32561, Abcam, Cambridge, UK), PERK (1:1000, #5683, Cell Signaling Technology, Danvers, MA, USA), eIF2α (1:1000, #9722, Cell Signaling Technology, Danvers, MA, USA), p-eIF2α (1:1000, #3398, Cell Signaling Technology, Danvers, MA, USA), ATF4 (1:1000, ab85049, Abcam, Cambridge, UK), CHOP (1:1000, #2895, Cell Signaling Technology, Danvers, MA, USA), and β-actin (1:1000, ab8226, Abcam, Cambridge, UK). The following day, membranes underwent three PBS washes followed by a 1-hour incubation at room temperature with Horseradish peroxidase (HRP)-conjugated secondary antibodies (goat anti-rabbit IgG, ab6721; goat anti-mouse IgG, ab6789; 1:5000, Abcam, Cambridge, UK). Protein signals were visualized using enhanced chemiluminescence (ECL) reagents (#32106, Thermo Fisher Scientific, Waltham, MA, USA) and imaged on a Tanon 5200 Multi imaging system (Tanon, Shanghai, China). Band intensities were quantified using ImageJ software (version 1.53, NIH, Bethesda, MD, USA).

Co-Immunoprecipitation (Co-IP)

Co-IP was conducted to assess Deltex E3 ubiquitin ligase 3L-tumor protein P53 (DTX3L-P53) interactions in RBE cells. Whole-cell lysates were incubated overnight at 4 °C with either DTX3L (1:100, ab70621, Abcam, Cambridge, UK) or P53 (1:100, ab26, Abcam, Cambridge, UK) antibodies bound to Protein A/G agarose beads (#9007, Cell Signaling Technology, Danvers, MA, USA) with gentle rotation. Following three washes to remove nonspecific proteins, the immunoprecipitates were resolved through SDS-PAGE and analyzed using Western blotting to examine the interaction of target proteins. To assess P53 ubiquitination, immunoprecipitates were probed with anti-ubiquitin antibody (1:1000, #3936, Cell Signaling Technology, Danvers, MA, USA), followed by incubation with HRP-conjugated secondary antibodies (goat anti-mouse IgG, ab6789; goat anti-rabbit IgG, ab6721; 1:5000, Abcam, Cambridge, UK). Signals were visualized using ECL reagents, and images were acquired on a Tanon 5200 Multi imaging system (Tanon, Shanghai, China). Protein band intensities and relative expression levels were determined using ImageJ software (version 1.53, NIH, Bethesda, MD, USA).

Assessment of P53 Protein Stability

To evaluate the stability of the P53 protein, RBE cells were treated with cycloheximide (CHX, #C7698, Sigma-Aldrich, St. Louis, MO, USA) to block *de novo* protein synthesis. At 0, 2, 4, and 8 hours after treatment, cells were harvested, and total protein was extracted using RIPA buffer containing protease inhibitors. Western blot analysis was performed to detect P53 levels at each time point. Blots were developed using ECL reagents and imaged on the Tanon 5200 Multi chemiluminescence imaging system (Tanon, Shanghai, China). Band intensities were quantified using ImageJ software (version 1.53, NIH, Bethesda, MD, USA) and normalized to the 0-hour time point sample to generate a degradation curve.

Statistical Analysis

Statistical analyses were conducted using SPSS version 23.0 (IBM Corp., Armonk, NY, USA). Data normality was examined using the Shapiro-Wilk test and variance homogeneity was assessed employing Levene's test. Quantitative data (continuous variables) were presented as mean $\pm$ standard deviation (SD). For comparisons between two groups, an independent samples *t*-test was used when parametric assumptions were met; otherwise, the Mann–Whitney U test was applied. Multiple-group comparisons were performed using one-way analysis of variance (ANOVA) coupled with Tukey's post hoc correction. However, if parametric assumptions were violated, the Kruskal–Wallis H test was employed. A *p*-value of less than 0.05 was considered statistically significant.

Results

Upregulation of DTX3L in Intrahepatic Cholangiocarcinoma

To evaluate DTX3L's expression levels in ICC, its mRNA levels were assessed in tumor tissues (ICC group) and paired adjacent normal (Normal group) using qRT-PCR. As shown in Fig. 1A, *DTX3L* was significantly upregulated in the ICC group compared to the Normal group ($p <$

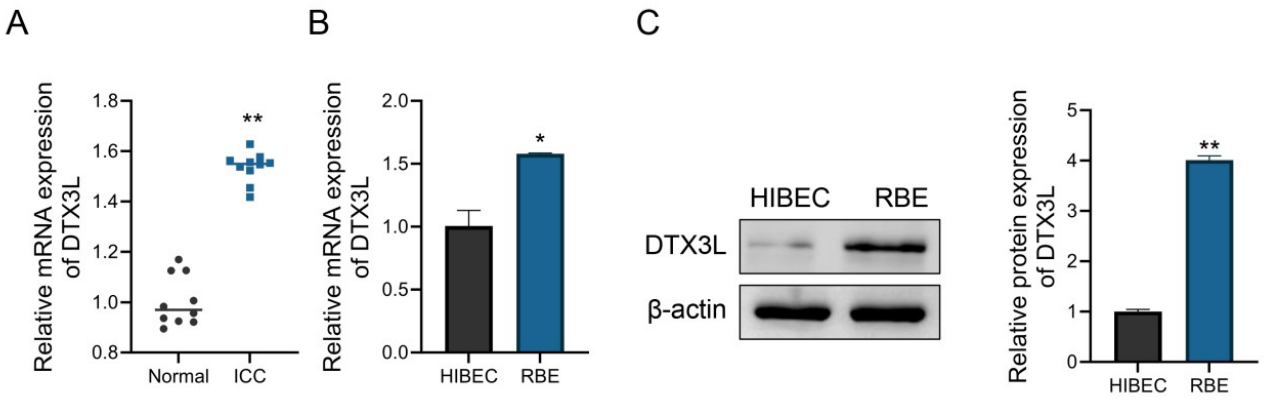

Fig. 1. Expression levels of DTX3L in intrahepatic cholangiocarcinoma. (A) qRT-PCR was used to assess DTX3L mRNA in the ICC and Normal groups (n = 10). (B) qRT-PCR analysis of DTX3L mRNA in HIBEC and RBE cells. (C) Western blot analysis of DTX3L protein in HIBEC and RBE cells. Data were presented as mean ± SD (n = 3). *$p < 0.05$, **$p < 0.01$ vs. Normal or HIBEC group. DTX3L, Deltex E3 ubiquitin ligase 3L; ICC, intrahepatic cholangiocarcinoma; HIBEC, human intrahepatic biliary epithelial cell; RBE, ICC cells; SD, standard deviation.

0.01), suggesting a critical role in the onset and progression of ICC. At the cellular level, qRT-PCR and Western blot analyses demonstrated that both DTX3L mRNA ($p < 0.05$) and protein ($p < 0.01$) were substantially higher in ICC cell line RBE compared to normal HIBECs (Fig. 1B,C).

These findings suggest that DTX3L was aberrantly upregulated in ICC and might contribute to tumor progression.

DTX3L Promoted ICC Cell Proliferation and Inhibited Apoptosis

Transfection efficiency was validated by qRT-PCR and Western blot analyses, demonstrating DTX3L overexpression and knockdown in RBE cells ($p < 0.01$, Fig. 2A,B). Functionally, DTX3L overexpression significantly enhanced cell viability and colony-forming ability ($p < 0.05$ or $p < 0.01$), whereas DTX3L knockdown exhibited the opposite effects ($p < 0.01$, Fig. 2C,D). TUNEL assay revealed reduced apoptosis in the oe-DTX3L group and increased apoptosis in the sh-DTX3L group ($p < 0.01$, Fig. 2E). Consistent with these results, Western blot analysis of apoptotic indicators showed that DTX3L overexpression upregulated Bcl-2 and downregulated Bax, Cleaved Caspase-3, and Cleaved PARP ($p < 0.01$), while DTX3L knockdown induced the opposite trends ($p < 0.01$, Fig. 2F).

These findings indicate that DTX3L promotes ICC cell proliferation and inhibits apoptosis.

DTX3L Negatively Regulated the Endoplasmic Reticulum Stress Pathway

As shown in Fig. 3, ERS-associated proteins (PERK, p-eIF2α, ATF4, and CHOP) were significantly upregulated in the sh-DTX3L group and downregulated in the oe-DTX3L group compared to their corresponding controls ($p < 0.01$). The expression of total eIF2α remained unchanged across all groups, suggesting that DTX3L regulates ERS primarily by modulating eIF2α phosphorylation. These results indicate that DTX3L is a negative regulator of the ERS response.

DTX3L Promoted Tumor Growth In Vivo

After 4 weeks of inoculation, tumor size and weight were measured in the oeNC, oe-DTX3L, shNC, and sh-DTX3L groups (Fig. 4A). Compared to the control group, tumor volume and weight were significantly increased in the oe-DTX3L group while significantly decreased in the sh-DTX3L group ($p < 0.05$, Fig. 4B,C). Tumor volume, measured every four days, revealed accelerated growth in the oe-DTX3L group and significant growth inhibition in the sh-DTX3L group ($p < 0.05$). Additionally, Western blot analysis of tumor tissues (Fig. 4D) demonstrated that DTX3L knockdown significantly upregulated P53 and ERS-related markers (PERK, p-eIF2α, ATF4, and CHOP), while DTX3L overexpression led to the opposite effect.

These observations suggest that DTX3L supports tumor growth by modulating P53 and ERS pathway.

Interaction Between DTX3L and P53

Western blot analysis (Fig. 5A) showed that DTX3L overexpression significantly reduced P53 protein levels ($p < 0.01$), whereas DTX3L knockdown increased P53 protein levels ($p < 0.01$), indicating that DTX3L modulated P53 expression. To assess P53 stability, RBE cells were treated with CHX, and the P53 degradation rate was examined over time (Fig. 5B). In the oe-DTX3L group, P53 degraded more rapidly ($p < 0.01$), however, in the sh-DTX3L group, P53 degradation was significantly delayed ($p < 0.05$ or $p < 0.01$), confirming that DTX3L promotes P53 stabil-

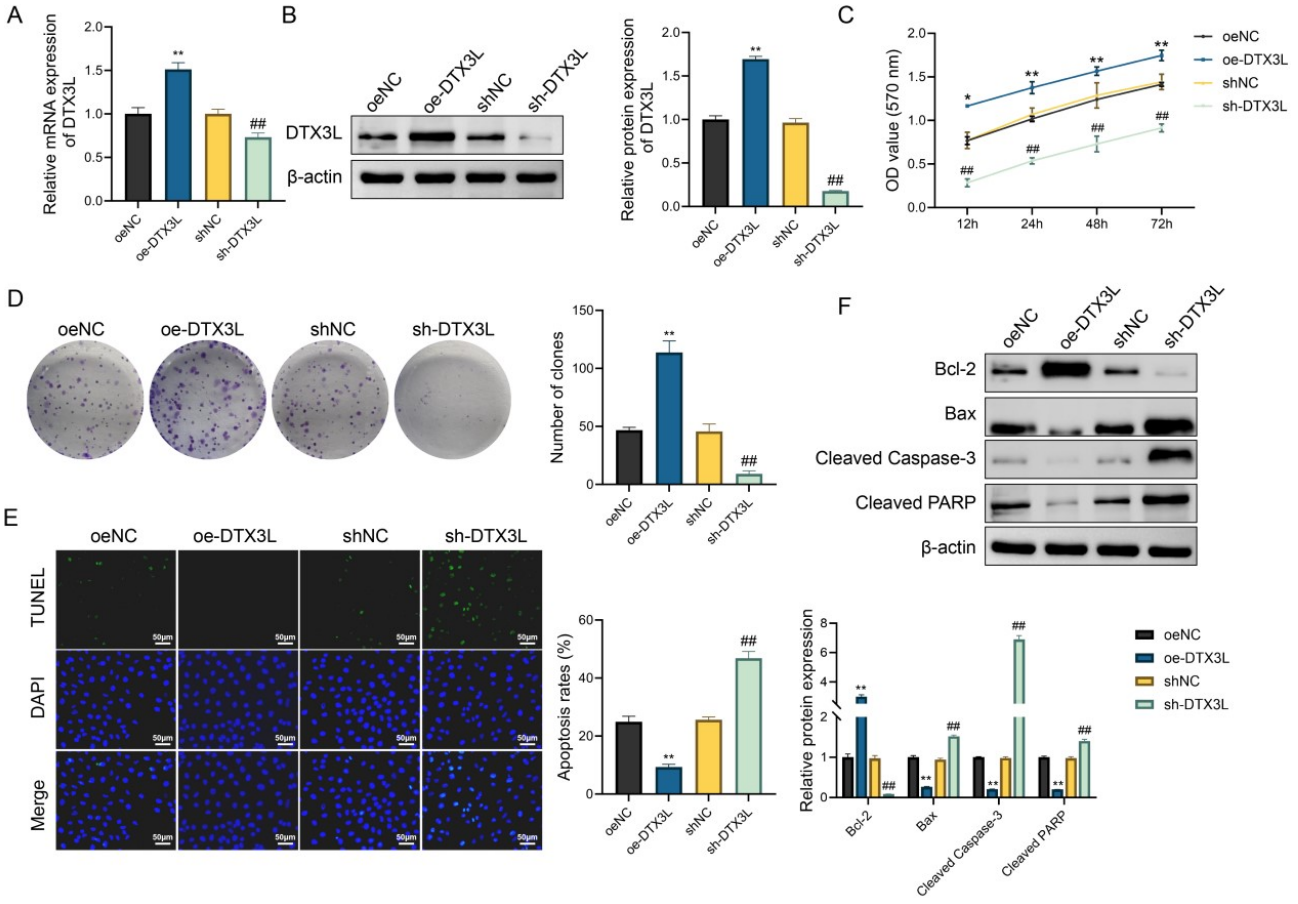

Fig. 2. DTX3L promoted ICC cell proliferation and inhibited apoptosis. (A) qRT-PCR analysis of DTX3L mRNA in RBE cells from the oeNC, oe-DTX3L, shNC, and sh-DTX3L groups. (B) Western blot analysis of DTX3L protein in RBE cells across the groups. (C) CCK-8 assay to detect the viability of RBE cells at various time points (12 h, 24 h, 48 h, 72 h) across the groups. (D) Colony formation assay to evaluate the colony-forming ability of RBE cells across the groups. (E) TUNEL assay to detect apoptosis in RBE cells across the groups. (F) Western blot analysis to assess Bcl-2, Bax, Cleaved Caspase-3 and Cleaved PARP in RBE cells. Data were presented as mean ± SD (n = 3). *$p < 0.05$, **$p < 0.01$ vs. oeNC group; $^{\#\#}p < 0.01$ vs. shNC group. CCK-8, Cell Counting Kit-8; TUNEL, Terminal deoxynucleotidyl transferase dUTP nick end labeling; DAPI, 4′,6-diamidino-2-phenylindole; PARP, Poly (ADP-ribose) polymerase.

ity. Furthermore, Co-IP assays (Fig. 5C) revealed a direct interaction between DTX3L and P53. Additionally, ubiquitination assays (Fig. 5D) showed that DTX3L overexpression significantly increased P53 ubiquitination ($p < 0.01$), promoting its degradation, whereas DTX3L knockdown decreased it ($p < 0.01$).

These findings collectively indicate that DTX3L binds to P53 and promotes its ubiquitin-mediated degradation, compromising P53 stability and function.

P53 Knockdown Reversed the Antitumor Effects of DTX3L Knockdown

Western blot analysis (Fig. 6A) demonstrated that DTX3L knockdown substantially increased P53 protein levels ($p < 0.01$), while simultaneous P53 knockdown reduced its expression ($p < 0.01$), confirming successful P53 suppression. Cell proliferation assays indicated that cell viability (Fig. 6B) and colony formation (Fig. 6C) were significantly reduced in the sh-DTX3L group ($p < 0.01$), but these proliferative capacities were significantly restored after P53 co-knockdown ($p < 0.05$). Apoptosis analysis using TUNEL staining (Fig. 6D) demonstrated an increase in apoptotic cells after DTX3L knockdown ($p < 0.01$), which was substantially rescued with P53 co-knockdown ($p < 0.01$). As shown in Fig. 6E, DTX3L knockdown significantly upregulated endoplasmic reticulum (ER) stress markers (p-eIF2α, PERK, CHOP, ATF4), but their level decreased substantially upon P53 co-knockdown ($p < 0.01$).

These findings indicate that P53 mediates the antitumor effects of DTX3L knockdown.

Discussion

This study investigated the role of DTX3L in ICC using both *in vitro* and *in vivo* models. We observed that DTX3L expression was significantly higher in ICC tissues

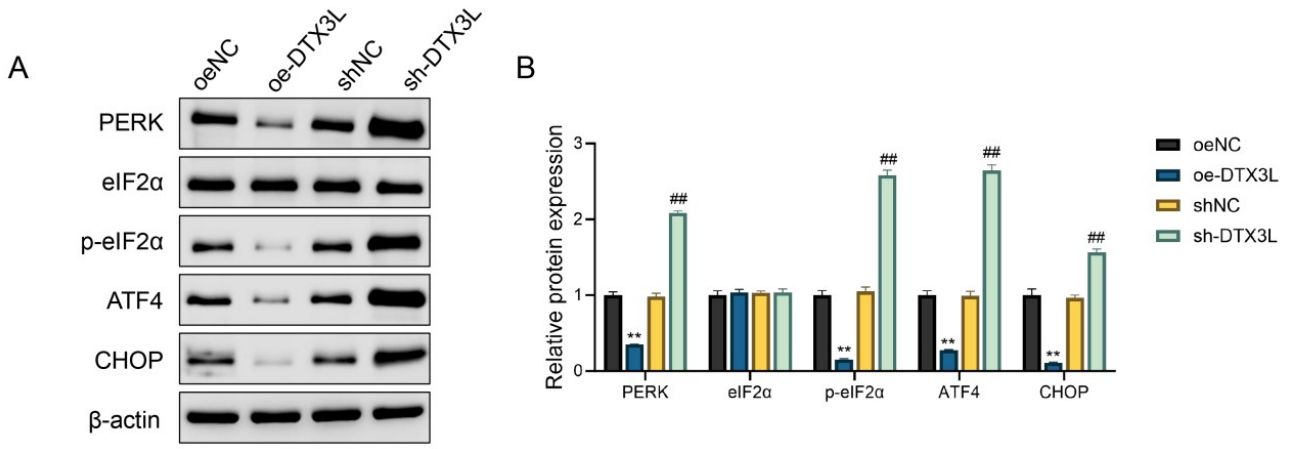

Fig. 3. DTX3L negatively regulated the endoplasmic reticulum stress response. (A) Representative protein bands of protein kinase R-like endoplasmic reticulum kinase (PERK), eukaryotic initiation factor 2 alpha (eIF2α), phosphorylated eIF2α (p-eIF2α), activating transcription factor 4 (ATF4), and C/EBP homologous protein (CHOP) in RBE cells from the oeNC, oe-DTX3L, shNC, and sh-DTX3L groups. (B) Relative expression levels of PERK, eIF2α, p-eIF2α, ATF4, and CHOP across all groups. Data were presented as mean ± SD (n = 3). $^{**}p < 0.01$ vs. oeNC group; $^{\#\#}p < 0.01$ vs. shNC group.

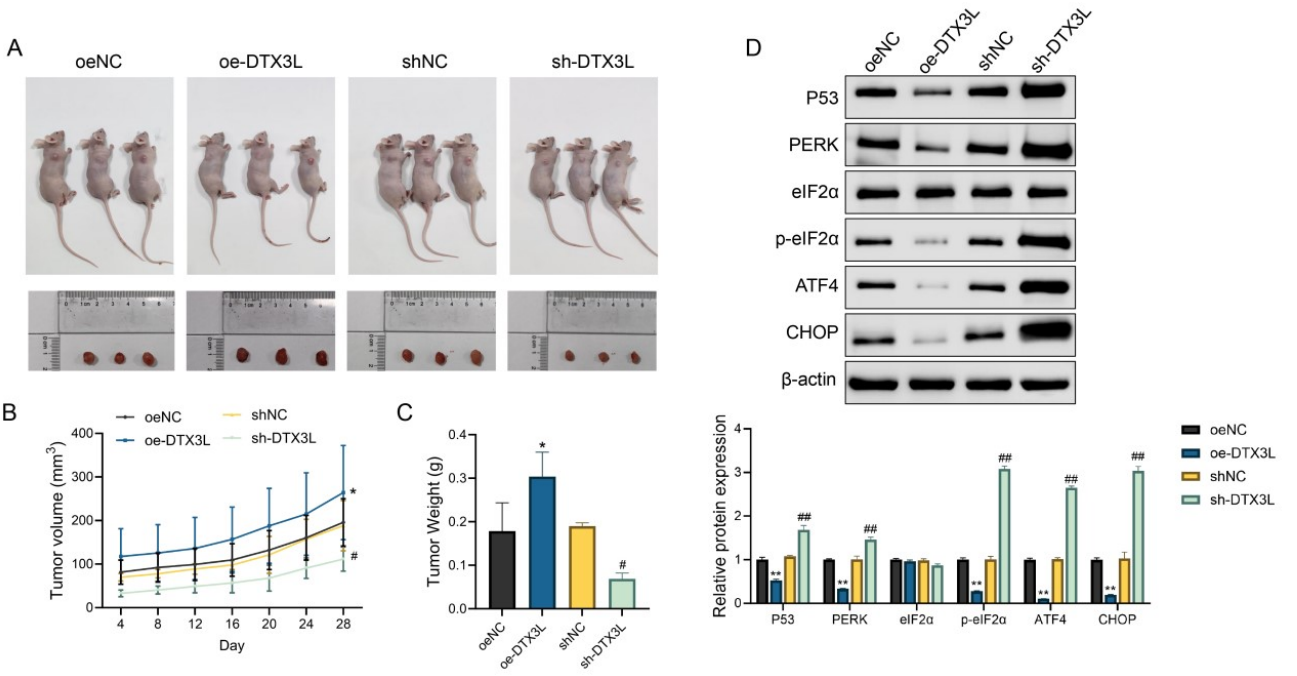

Fig. 4. DTX3L promoted tumor growth *in vivo*. (A) Visual representation of tumors harvested from mice in the oeNC, oe-DTX3L, shNC, and sh-DTX3L groups. (B) Tumor volumes of mice across the groups over 28 days. (C) Tumor weight comparison for mice across the groups upon study completion. (D) Western blot analysis of P53, PERK, eIF2α, p-eIF2α, ATF4, and CHOP protein levels in tumor tissues from the four groups. Data were presented as mean ± SD (n = 3). $^{*}p < 0.05$, $^{**}p < 0.01$ vs. oeNC group; $^{\#}p < 0.05$, $^{\#\#}p < 0.01$ vs. shNC group.

and cell lines compared to normal controls, promoting tumor progression by enhancing cell proliferation, inhibiting apoptosis, and regulating the ERS pathway. Furthermore, DTX3L directly interacted with P53 and accelerated its ubiquitination-mediated degradation, thereby impairing its tumor-suppressive function. In *in vivo* models, DTX3L knockdown significantly suppressed tumor growth, which was reversed when P53 was simultaneously knockdown. These findings suggest that DTX3L might act as a critical regulator of ICC progression and highlight its potential as a therapeutic target.

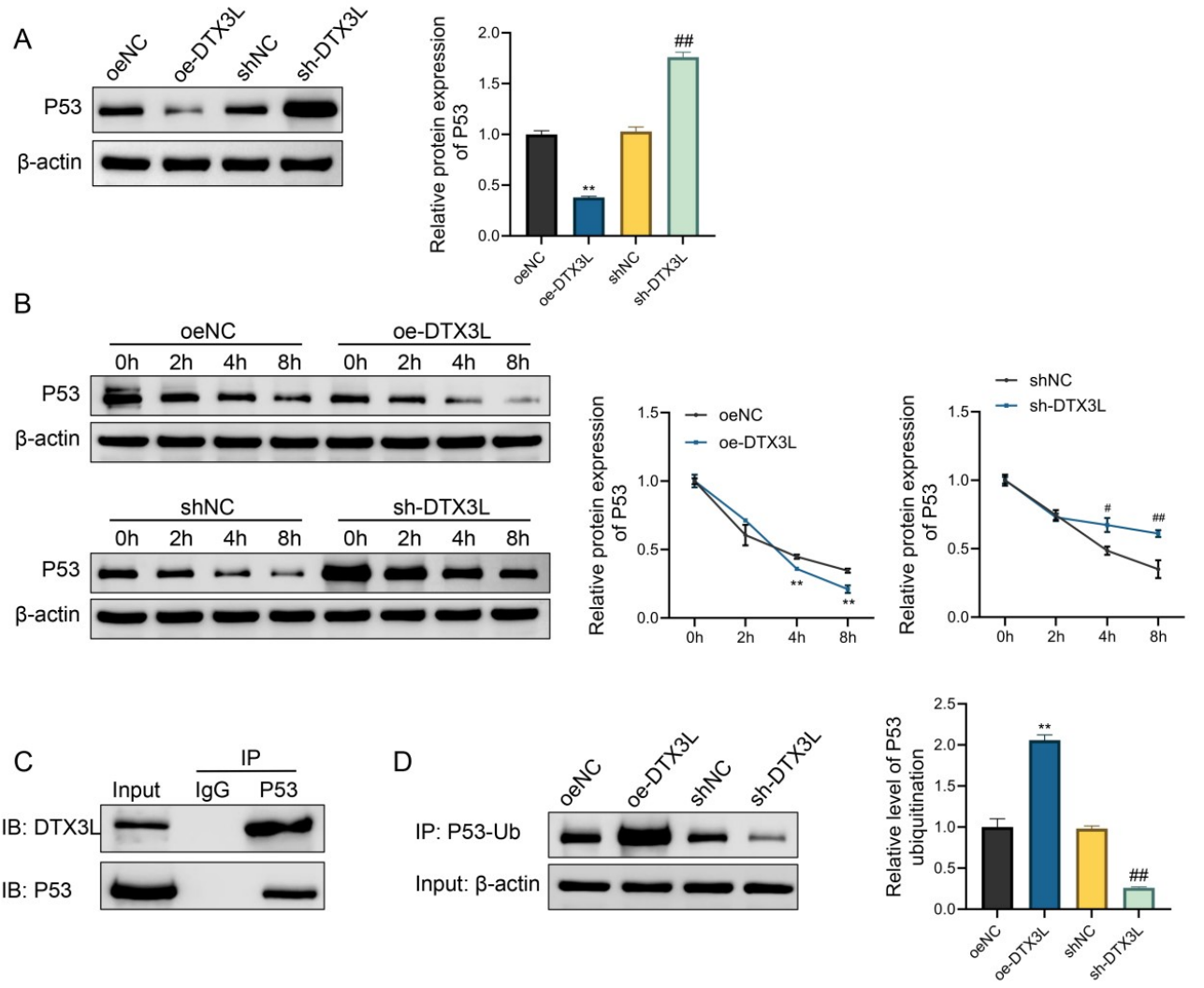

Fig. 5. Interaction between DTX3L and P53. (A) Western blot analysis of P53 protein levels in RBE cells from the oeNC, oe-DTX3L, shNC, and sh-DTX3L groups. (B) P53 protein levels in RBE cells from each group after 0, 2, 4, and 8 hours of treatment with CHX. (C) Co-IP assay to determine the binding between DTX3L and P53 in RBE cells. (D) Co-IP was followed by immunoblotting to assess the ubiquitination levels of P53 in RBE cells from each group. β-actin was used as a loading control in the input samples. Data were expressed as mean ± SD (n = 3). $^{**}p < 0.01$ vs. oeNC group; $^{\#}p < 0.05$, $^{\#\#}p < 0.01$ vs. shNC group. CHX, cycloheximide; Co-IP, Co-Immunoprecipitation.

This study provides novel evidence supporting the oncogenic function of DTX3L in ICC. As an E3 ubiquitin ligase, DTX3L's pro-tumorigenic effects have been widely reported in various cancers [19]. For example, DTX3L enhances breast cancer cell proliferation by promoting the ubiquitination and degradation of tumor suppressors [21,22]. Nevertheless, the precise functions and regulatory pathways of DTX3L in ICC remain poorly understood. Our findings bridge this knowledge gap by elucidating the molecular mechanism through which DTX3L promotes ICC progression, offering crucial theoretical insights into its oncogenic functions.

P53, a crucial tumor suppressor, is tightly modulated by various ubiquitination pathways [8]. Our findings confirm DTX3L's pivotal role in the ubiquitination-mediated P53 degradation, as evidenced by the direct interaction between DTX3L and P53, leading to accelerated P53 degradation. In addition to destabilizing P53, DTX3L significantly suppressed P53-mediated ERS signaling. Notably, ERS participates in cancer progression with dual functionality, either suppressing tumors by enhancing apoptosis or supporting tumor cell survival by adaptive stress responses [12,23,24]. We found that increased DTX3L expression effectively reduced pro-apoptotic ERS signaling activated by P53, thereby enhancing ICC cell proliferation. These results contribute to our understanding of P53 regulation and highlight mechanisms of stress modulation in the tumor microenvironment.

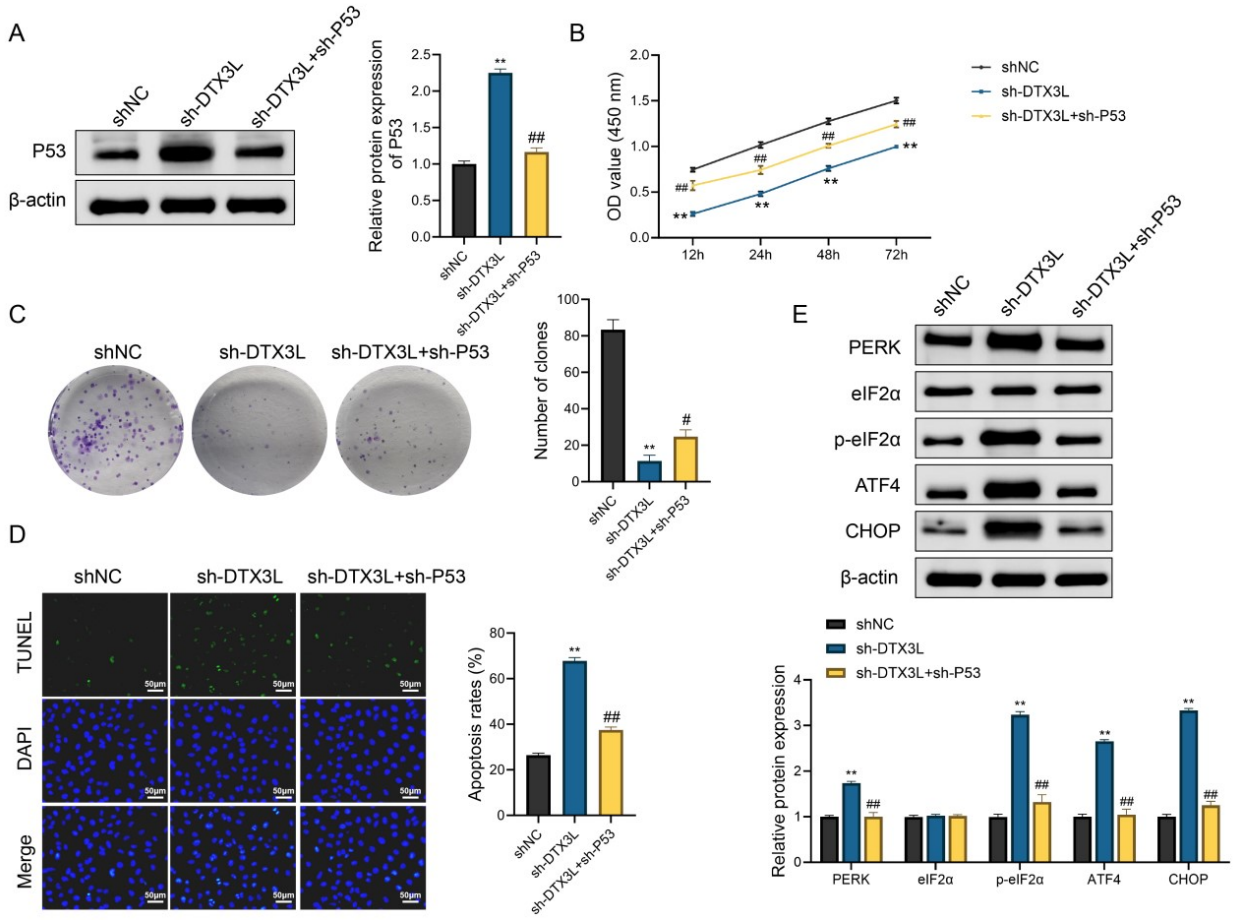

Fig. 6. P53 knockdown reversed the antitumor effects of DTX3L knockdown. (A) Western blot analysis of P53 in RBE cells from the shNC, sh-DTX3L, and sh-DTX3L+sh-P53 groups. (B) CCK-8 assay to examine RBE cell viability across the groups. (C) Colony formation experiment to evaluate the colony-forming ability of RBE cells across the groups. (D) TUNEL assay to assess RBE cell apoptosis levels across the groups. (E) Western blot analysis to quantify PERK, eIF2α, p-eIF2α, ATF4, and CHOP in RBE cells across the groups. Data were presented as mean ± SD (n = 3). $^{**}p < 0.01$ vs. shNC group; $^{\#}p < 0.05$, $^{\#\#}p < 0.01$ vs. sh-DTX3L group.

ICC is characterized by high aggressiveness and its ability to adapt to a hostile microenvironment, which distinguishes it from other cancers [25]. In this context, DTX3L's role in regulating both P53 stability and ERS is particularly significant. This study, through *in vitro* cell experiments and *in vivo* animal models, confirmed the critical role of DTX3L in ICC tumor progression. Notably, in animal experiments, DTX3L knockdown significantly inhibited tumor volume and weight while increasing the expression of ER stress markers (PERK, p-eIF2α, ATF4, and CHOP), further validating the role of restored P53 function in promoting ER stress and apoptosis. Conversely, DTX3L overexpression significantly reduced both P53 and ER stress-proteins, further supporting its role in facilitating ICC progression through ubiquitin-mediated degradation of P53.

Despite the compelling findings, we acknowledge several limitations in this study. First, the research primarily relied on *in vitro* assays and subcutaneous xenograft models, which may not fully capture the complexity of the human tumor microenvironment. Second, while P53 was identified as a key substrate of DTX3L-mediated ubiquitination, the potential involvement of other oncogenic targets (such as phosphatase and tensin homolog (PTEN) or forkhead box O (FOXO)) was not explored, warranting ubiquitinome-wide proteomic analyses and competitive assays to determine additional substrates. Third, although DTX3L knockdown activated ERS and promoted apoptosis, the lack of pathway-specific inhibitors (e.g., the PERK inhibitor GSK2606414) prevents us from establishing direct causality. Fourth, blank control groups were not included in certain functional assays, which may have affected the robustness of internal comparisons. Finally, the relatively limited number of clinical samples restricts the generalizability of our results. Future investigations should expand clinical validation cohorts, incorporate ER stress inhibitors, implement comprehensive experimental controls, and explore DTX3L's interaction with broader signaling networks to better explain its tumorigenic and therapeutic role in ICC and other malignancies.

Conclusion

This study reveals that DTX3L serves as a key oncogenic factor in ICC by promoting the ubiquitination-mediated degradation of P53, thereby suppressing ERS and apoptosis. These findings provide novel insights into the molecular mechanisms underlying ICC and establish a theoretical foundation for targeting DTX3L as a novel therapeutic approach.

Availability of Data and Materials

The datasets used and/or analyzed during the current study are available from the corresponding authors on reasonable request.

Author Contributions

HL, JH, SY, LH, XS, MZ and GZ contributed to the study conception and design. SY, LH, XS, and MZ were responsible for material preparation, data collection, and analysis. The first draft of this manuscript was written by HL, JH and GZ. All authors contributed to the critical revision of the manuscript for important intellectual content. All authors read and approved the final manuscript and agree to be accountable for all aspects of the work in ensuring the accuracy and integrity of any part of the work.

Ethics Approval and Consent to Participate

All human tissue collection procedures adhered to the Declaration of Helsinki and written informed consent was obtained from each patient prior to participation. This research received ethical approval from the Ethics Committee of Taihe Hospital, Hubei University of Medicine (Approval No. SYLC1025). All animal procedures followed the reporting of *In Vivo* Experiments (ARRIVE) guidelines and were approved by the Institutional Animal Care and Use Committee (IACUC) of Taihe Hospital, Hubei University of Medicine (Approval No. SY-KY20250105).

Acknowledgment

Not applicable.

Funding

This research received no external funding.

Conflict of Interest

The authors declare no conflict of interest.

References

[1] Cai T, Dai J, Lin Y, Bai Z, Li J, Meng W. N-acetyltransferase 10 affects the proliferation of intrahepatic cholangiocarcinoma and M2-type polarization of macrophages by regulating C-C motif chemokine ligand 2. Journal of Translational Medicine. 2024; 22: 875. https://doi.org/10.1186/s12967-024-05664-z.

[2] Qin D, Chen J, Tang Y, Li Z, Geng Z, Wu H, *et al*. Evaluation of the outcomes of staging laparoscopy in intrahepatic cholangiocarcinoma patients undergoing surgical resection: a multicenter retrospective study in China. Hepatoma Research. 2024; 10: 40. http://dx.doi.org/10.20517/2394-5079.2024.65.

[3] Jiang JH, Fang DZ, Hu YT. Influence of surgical margin width on survival rate after resection of intrahepatic cholangiocarcinoma: a systematic review and meta-analysis. BMJ Open. 2023; 13: e067222. https://doi.org/10.1136/bmjopen-2022-067222.

[4] Yu TH, Chen X, Zhang XH, Zhang EC, Sun CX. Clinicopathological characteristics and prognostic factors for intrahepatic cholangiocarcinoma: a population-based study. Scientific Reports. 2021; 11: 3990. https://doi.org/10.1038/s41598-021-83149-5.

[5] Chen X, Du J, Huang J, Zeng Y, Yuan K. Neoadjuvant and Adjuvant Therapy in Intrahepatic Cholangiocarcinoma. Journal of Clinical and Translational Hepatology. 2022; 10: 553–563. https://doi.org/10.14218/JCTH.2021.00250.

[6] Dai YS, Hu HJ, Lv TR, Hu YF, Zou RQ, Li FY. The influence of resection margin width in patients with intrahepatic cholangiocarcinoma: a meta-analysis. World Journal of Surgical Oncology. 2023; 21: 16. https://doi.org/10.1186/s12957-023-02901-5.

[7] Wang H, Guo M, Wei H, Chen Y. Targeting p53 pathways: mechanisms, structures, and advances in therapy. Signal Transduction and Targeted Therapy. 2023; 8: 92. https://doi.org/10.1038/s41392-023-01347-1.

[8] Zou T, Lin Z. The Involvement of Ubiquitination Machinery in Cell Cycle Regulation and Cancer Progression. International Journal of Molecular Sciences. 2021; 22: 5754. https://doi.org/10.3390/ijms22115754.

[9] Wang J, Liu W, Zhang L, Zhang J. Targeting mutant p53 stabilization for cancer therapy. Frontiers in Pharmacology. 2023; 14: 1215995. https://doi.org/10.3389/fphar.2023.1215995.

[10] Toma-Fukai S, Shimizu T. Structural Diversity of Ubiquitin E3 Ligase. Molecules (Basel, Switzerland). 2021; 26: 6682. https://doi.org/10.3390/molecules26216682.

[11] Du X, Song H, Shen N, Hua R, Yang G. The Molecular Basis of Ubiquitin-Conjugating Enzymes (E2s) as a Potential Target for Cancer Therapy. International Journal of Molecular Sciences. 2021; 22: 3440. https://doi.org/10.3390/ijms22073440.

[12] Zhang W, Shi Y, Oyang L, Cui S, Li S, Li J, *et al*. Endoplasmic reticulum stress-a key guardian in cancer. Cell Death Discovery. 2024; 10: 343. https://doi.org/10.1038/s41420-024-02110-3.

[13] Song Y, Ma J, Fang L, Tang M, Gao X, Zhu D, *et al*. Endoplasmic reticulum stress-related gene model predicts prognosis and guides therapies in lung adenocarcinoma. BMC Bioinformatics. 2023; 24: 255. https://doi.org/10.1186/s12859-023-05384-z.

[14] Wadgaonkar P, Wang Z, Chen F. Endoplasmic reticulum stress responses and epigenetic alterations in arsenic carcinogenesis. Environmental Pollution (Barking, Essex: 1987). 2024; 347: 123565. https://doi.org/10.1016/j.envpol.2024.123565.

[15] Li Q, Zhao X, Yang H, Zhu X, Sui X, Feng J. Modulating Endoplasmic Reticulum Stress in Gastrointestinal Cancers: Insights from Traditional Chinese Medicine. Pharmaceuticals (Basel, Switzerland). 2024; 17: 1599. https://doi.org/10.3390/ph17121599.

[16] Zhang JX, Yuan WC, Li CG, Zhang HY, Han SY, Li XH. A review on the mechanisms underlying the antitumor effects of natural products by targeting the endoplasmic reticulum stress apoptosis pathway. Frontiers in Pharmacology. 2023; 14: 1293130. https://doi.org/10.3389/fphar.2023.1293130.

[17] Yan Q, Ding J, Khan SJ, Lawton LN, Shipp MA. DTX3L E3 ligase targets p53 for degradation at poly ADP-ribose polymerase-

associated DNA damage sites. iScience. 2023; 26: 106444. https://doi.org/10.1016/j.isci.2023.106444.

[18] Hu W, Hu Y, Pei Y, Li R, Xu F, Chi X, *et al*. Silencing DTX3L Inhibits the Progression of Cervical Carcinoma by Regulating PI3K/AKT/mTOR Signaling Pathway. International Journal of Molecular Sciences. 2023; 24: 861. https://doi.org/10.3390/ijms24010861.

[19] Wang L, Sun X, He J, Liu Z. Functions and Molecular Mechanisms of Deltex Family Ubiquitin E3 Ligases in Development and Disease. Frontiers in Cell and Developmental Biology. 2021; 9: 706997. https://doi.org/10.3389/fcell.2021.706997.

[20] Chun YS, Pawlik TM, Vauthey JN. 8th Edition of the AJCC Cancer Staging Manual: Pancreas and Hepatobiliary Cancers. Annals of Surgical Oncology. 2018; 25: 845–847. https://doi.org/10.1245/s10434-017-6025-x.

[21] Mirzalieva O, Juncker M, Schwartzenburg J, Desai S. ISG15 and ISGylation in Human Diseases. Cells. 2022; 11: 538. https://doi.org/10.3390/cells11030538.

[22] Revici R, Hosseini-Alghaderi S, Haslam F, Whiteford R, Baron M. E3 Ubiquitin Ligase Regulators of Notch Receptor Endocytosis: From Flies to Humans. Biomolecules. 2022; 12: 224. https://doi.org/10.3390/biom12020224.

[23] Wu J, Qiao S, Xiang Y, Cui M, Yao X, Lin R, *et al*. Endoplasmic reticulum stress: Multiple regulatory roles in hepatocellular carcinoma. Biomedicine & Pharmacotherapy. 2021; 142: 112005. https://doi.org/10.1016/j.biopha.2021.112005.

[24] Qing B, Wang S, Du Y, Liu C, Li W. Crosstalk between endoplasmic reticulum stress and multidrug-resistant cancers: hope or frustration. Frontiers in Pharmacology. 2023; 14: 1273987. https://doi.org/10.3389/fphar.2023.1273987.

[25] Wei P, Li Z. Advancing immunotherapy for intrahepatic cholangiocarcinoma: exploring the tumor immune microenvironment and innovative treatments. Hepatoma Research. 2024; 10: 39. http://dx.doi.org/10.20517/2394-5079.2024.72.